Magnetic Resonance Imaging versus Computed Tomography for Biliary Tract Intraductal Papillary Mucinous Neoplasm (BT-IPMN): A Diagnostic Performance Analysis

Authors' Contribution:		
Study Design A	BCF 1	Jing Li
Data Collection B	ACF 1	Yuanlin Yu
Statistical Analysis C	ABCF 1	Lulong Zhu
Data Interpretation D	ABDF 1	Yuping Li
Manuscript Preparation E	BEF 2	Qing He
Literature Search F		
Funds Collection G		

1 Department of Medical Imaging, The First Affiliated Hospital of Fujian Medical University, Fuzhou, Fujian, P.R. China
2 Department of Radiology, The First Affiliated Hospital of Fujian Medical University, Fuzhou, Fujian, P.R. China

Corresponding Author: Qing He, e-mail: TaniaRileykby@yahoo.com
Source of support: Departmental sources

Background: In most cases, biliary tract intraductal papillary mucinous neoplasm (BT-IPMN) is depicted by pathological features rather than on imaging modalities, but fine-needle aspiration cytology cannot provide complete information on tumor(s). Computed tomography (CT) has the advantage of high spatial resolution and multiplanar capabilities, while magnetic resonance imaging (MRI) has greater contrast resolution than CT. The purpose of this study was to compare the diagnostic performance of CT *vs*. MRI for the diagnosis of BT-IPMN using surgical pathology as the reference standard.

Material/Methods: Data from CT, MRI, and surgical pathology of 210 patients with complaints of abdominal discomfort, vomiting, and/or jaundice for at least 6 months were included in the analysis. Intra-observer agreements for diagnosis of neoplasm was evaluated by *kappa* statistics.

Results: CT and MRI respectively detected 171 and 33 patients with BT-IPMN, 6 and 176 with biliary intraductal tubulo-papillary neoplasms (BT-ITPN), and 28 and 6 with inconclusive results. Surgical pathology reported 179 patients with BT-IPMN and 25 patients with BT-ITPN. CT and MRI both had the same accuracy (97.14%) for BT-IPMN. The sensitivities for diagnosis of BT-IPMN were 87.75%, 83.81%, and 81.43% for the surgical pathology, MRI, and CT, respectively. Intra-observer agreements for diagnosis of neoplasm were substantial (k=0.79), perfect (k=0.81), and perfect (k=0.85) for CT, MRI, and surgical pathology, respectively.

Conclusions: MRI appears to be a more accurate and reliable method than CT for depicting BT-IPMN.

MeSH Keywords: Abdominal Neoplasms • Bile Duct Neoplasms • Biliary Tract Neoplasms • Magnetic Resonance Imaging • Tomography, Emission-Computed

Abbreviations: **BT-IPMN** – biliary tract intraductal papillary mucinous neoplasm; **CT** – computed tomography; **MRI** – magnetic resonance imaging; **STROBE** – the strengthening the reporting of observational studies in epidemiology; **3-D** – three-dimensional; **BT-ITPN** – biliary intraductal tubulopapillary neoplasms; k – *kappa* coefficient; **ICC** – intraclass correlation coefficient; **FDG PET/CT** – fluorodeoxyglucose/positron emission tomography/computed tomography

Full-text PDF: https://www.medscimonit.com/abstract/index/idArt/920952

📄 2418   📊 3   📈 5   📖 16

CLINICAL RESEARCH

Background

Biliary tract intraductal papillary mucinous neoplasm (BT-IPMN) is a mucinous and papillary neoplasm found in the biliary epithelium and has diffuse intraductal or solitary growth [1]. It is very rare, presents in the intra- and extra-hepatic biliary tract, and is characterized by mucin-secreting cystic and/or papillary lesions [2]. It is the precursor of invasive carcinoma (tubular adenocarcinoma/mucinous carcinoma) and has a 40–80% chance of having invasive components in its surgical pathology [3]. Compared with conventional cholangiocarcinoma, it has a more favorable prognosis [2]. Surgery is the treatment of choice [4].

In most cases, BT-IPMN is defined by pathological description rather than by imaging findings [5], but fine-needle aspiration cytology cannot provide complete information about the tumor(s) [6]. Computed tomography (CT) has the advantage of high spatial resolution and multiplanar capabilities [7], while magnetic resonance imaging (MRI) has greater contrast resolution than CT, which makes it possible to detect biliary extensions [8]. CT and MRI are successful in showing anatomical features of BT-IPMN [6].

The purpose of this retrospective study was to compare the diagnostic performance of CT *vs.* MRI in the diagnosis of BT-IPMN using surgical pathology as the reference standard.

Material and Methods

Ethics consideration and consent to participate

The protocol (FMU/CL/18/19 dated 30 August 2019) of the study was approved by the Fujian Medical University review board. The reporting adheres to the law of China, strengthening the reporting of observational studies in epidemiology (STROBE) statement: Cross-sectional studies, and the 2008 Helsinki Declaration. All the enrolled patients signed an informed consent form regarding pathology, radiology, anesthesia (if required), surgeries (if required), and publication of the study, including personal images and data in all forms of publications (hard and/or electronics) irrespective of time and language during hospitalization.

Study population

During the period from 15 January 2006 to 25 August 2019, a total of 248 patients were available in the Department of Gastroenterology of the First Affiliated Hospital of Fujian Medical University (Fuzhou, China) and Department of Radiology, Zhongshan Hospital, Fudan University (Shanghai, China) and the referring hospitals with complaints of abdominal discomfort, recurrent upper abdominal pain, vomiting, weight loss, jaundice, and/or nausea for at least 6 months. Among them, 5 patients had not undergone pre-operative hepatic CT or MRI, 13 patients received pre-operative radiotherapy, 14 patients received pre-operative chemotherapy, and complete data of 6 patients were not available in the records of institutes. Therefore, data on these patients were not included in the final analysis. The data on 210 patients were included for analysis (Figure 1).

### Hepatic computed tomography examinations

Hepatic CT was performed using a 64-sliced scanner (Toshiba, Tokyo, Japan). Water was used as an oral contrast agent. We injected 120 mL of contrast agent (Meglumin diatrizoate, Xudonghaipu Co. Ltd, Shanghai, China) with a 20G angiocatheter (the Medrad power injection system, Bayer Healthcare, Berlin, Germany) into the antecubital vein at a rate of 2–5 mL/s, followed by a triple-phase CT. The arterial, venous, and decay phases were obtained at 30 s, 60 s, and 180 s, respectively, after administration of contrast agent. The imaging protocols were: 64×0.6 mm detector collimation, 120 kVp, 3-mm slice thickness, 200–250 mAs, and 3-mm slice intervals [6]. Radiologists (minimum 3 years of experience in abdominal imaging, blinded regarding MRI) performed the hepatic CT imaging.

Analysis of computed tomography images

All CT images were uploaded to a workstation (AW4.3, GE Healthcare, Chicago, IL, USA) for image analyses. In all images, the presence or absence of dilatation of the bile duct (a bile duct diameter >2 mm or the adjacent portal vein diameter >40% was considered as the dilatation of upstream bile duct and a common duct diameter >8 mm was considered as the dilatation of downstream bile duct [9]), the location of neoplasm, and the presence/absence of intraductal material(s) were evaluated. If intraductal material was present, we evaluated the height (the perpendicular distance from the tip of the material to the base) and length of the bile duct, and the presence/absence of the intense enhancement rim at the base of the material. The contrast-enhanced hepatic parenchyma was categorized as hypodense, isodense, or hyperdense. If intraductal material was not present, the thickening of the bile duct was evaluated. We also evaluated the type of margin at the base of the material where an intense enhancement rim was found (smooth, irregular, or bulging) and the presence/absence of vascular invasion, parenchymal atrophy, abscess, and stone [7]. Radiologists (minimum 10 years of experience in abdominal imaging, blinded regarding MRI) were involved in image analyses.

Hepatic magnetic resonance imaging examinations

Hepatic MRI was performed using a 3.0 Tesla scanner (Siemens AG, Munich, Germany) using a surface phased-array coil.
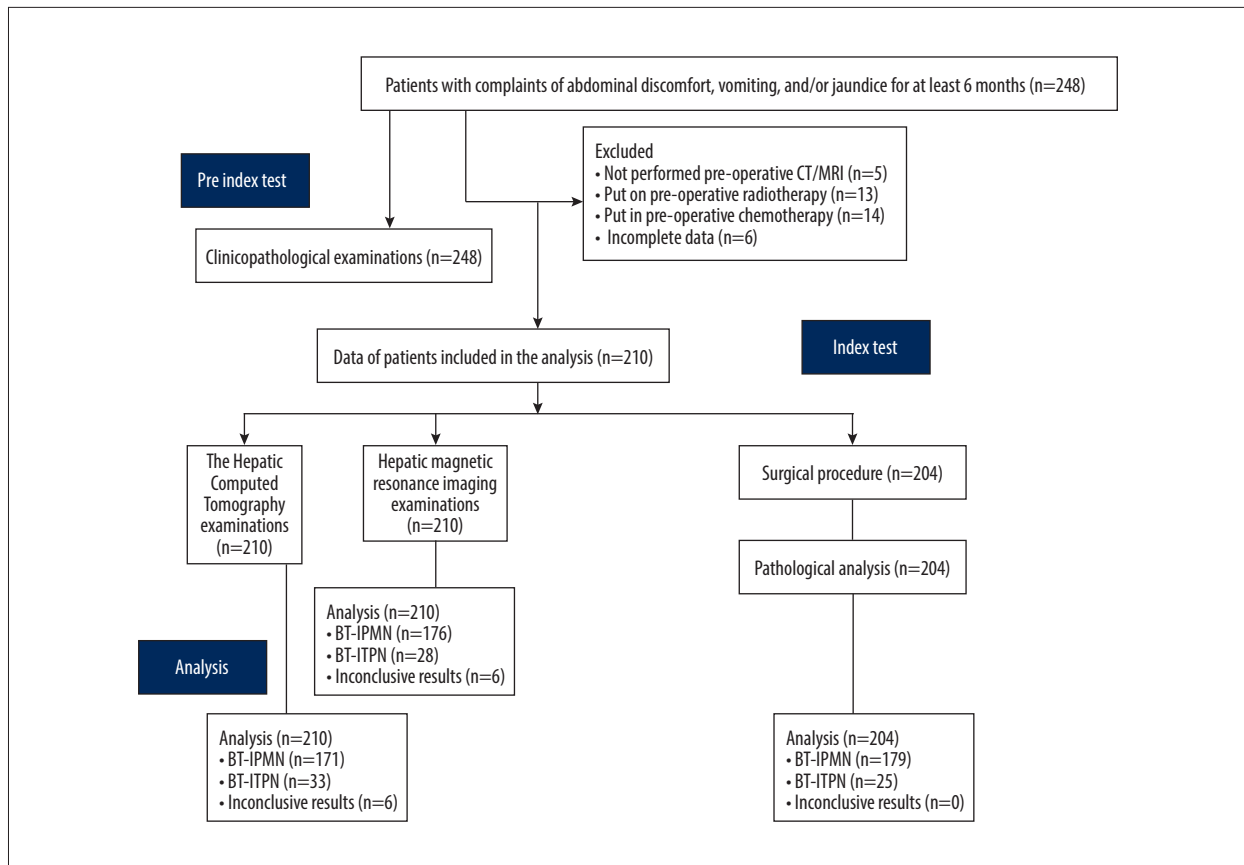
Figure 1. Flow diagram of the study.

All patients underwent three-plane scout view acquisition, T1-weighted unenhanced images, T2-weighted unenhanced images, diffused weighted images, and magnetic resonance cholangiopancreatography [6]. We injected 0.1 mM/kg gado-pentetate dimeglumine (Magnevist; Bayer Healthcare, Berlin, Germany) at the rate of 1–3 mL/s, and fat-saturated contrast-enhanced MRI was performed (T1-weighted sequences) 20 min later [4]. The imaging protocols were: 256×256 matrix size, 22×22 cm the field of view, and 750 ms echo time [6]. Radiologists (minimum 3 years of experience in abdominal imaging) performed hepatic MRI.

Analysis of magnetic resonance imaging

MR images were uploaded to the picture archiving and communication system workstation (SYNAPSE (PACS), 3.1.1., Fujifilm (China) Investment Co., Shanghai, China) for image analyses. In all images, we evaluated the presence or absence of crimping of the liver capsule (flattening, or concavities of the convex border and/or focal irregularities of the liver capsule [10]), atrophy of the liver parenchyma (reduced size of the corresponding liver lobe by at least 50%), the upstream bile duct dilatation (a bile duct diameter >2 mm or the adjacent portal vein diameter > 40%), enhancement of the peribiliary liver parenchyma, the proportion of intraductal soft tissue, and tumor location. To determine intraductal tumor volume, the tumor area or area of interest was described on each imaging slice of the axial MR image. For determination of the total volume of the intrahepatic dilated duct, the dilated ductal area or area of interest was described on each imaging slice of the axial MR image. The 3-D tumor volume and the total volume of the intrahepatic dilated duct were calculated by multiplying slice profile by the intraductal tumor volume and by the total volume of the intrahepatic dilated duct. The intraductal soft tissue proportion was calculated as the ratio of intraductal tumor volume to the total intrahepatic dilated ductal volume [5]. Radiologists (minimum 10 years of experience in abdominal imaging) were involved in image analyses.

Surgical procedure

In supine or lateral decubitus position, laparoscopy was performed and nodule(s) were resected using a harmonic scalpel (Harmonic G-300; Ethicon, Sommerville, NJ, USA) under general anesthesia, then the resected sample was sent to pathology [11]. Gastroenterologists (minimum 3 years of experience in abdominal surgeries) performed the surgeries.

CLINICAL RESEARCH

Pathological analysis

In the pathology laboratory, the samples were treated, slides were prepared and examined under a light microscope (Olympus, Beijing, China). A mucinous and papillary neoplasm originated from biliary epithelium with isolated/dilated intraductal growths were treated as BT-IPMN [1]. Pathologists (minimum 3 years of experience; blinded regarding CT and MRI results) performed the histopathology examination.

Beneficial score analysis

The beneficial score analysis for each modality was evaluated as per Eq. 1:

$$\text{Beneficial score} = \frac{\dfrac{\text{True BT-IPMN detected}}{\text{The numbers of samples analyzed}} - \dfrac{\text{BT-IPMN detected instead of BT-IPMN}}{\text{The numbers of samples analyzed}}}{\dfrac{\text{The level of diagnostic confidence above which surgery was performed}}{1 - \text{The level of diagnostic confidence above which surgery was performed}}} \times \quad (1)$$

Statistical analysis

All statistical analyses were performed by InStat 3.1 (GraphPad, San Diego, CA, USA). The chi-square independence test was performed for categorical data and the Mann-Whitney U test was performed for continuous data [5]. All results were considered significant at a 95% level of confidence. Intra-observer agreements for diagnosis of neoplasm, evaluation of either BT-IPMN or biliary intraductal tubulopapillary neoplasms (BT-ITPN), and numbers of lesions were evaluated by *kappa* statistics. A *kappa* coefficient (*k*) value, decoded as 0.99–0.81, indicated perfect agreement, 0.80–0.61 indicated substantial agreement, 0.60–0.41 indicated moderate agreement, 0.40–0.21 indicated fair agreement, and 0.20–0.01 indicated slight agreement [6]. Intra-observer agreements for the size of neoplasm were evaluated by the Bland-Altman plot method. The intraclass correlation coefficient (ICC), decoded as 1.00–0.91, was regarded as excellent, 0.90–0.81 as very good, and 0.80–0.71 as good [12].

Results

Clinical findings

The enrolled patients had either chronic or acute cholangitis. Patients had a mean age of 58.25±6.45 years (range, 35–72 years). Most of the patients had abdominal discomfort and nausea. Clinicopathological parameters also showed abnormally elevated levels of bile parameters. The detailed clinicopathological characteristics and physical examination of the patients are shown in Table 1.

Table 1. Demographical parameters, clinicopathological characteristics, and physical symptoms of the enrolled patients.

Parameters		Value	
Patients		210	
Age (years)	Minimum	35	
	Maximum	72	
	Mean±SD	58.25±6.45	
Sex	Male	95	(45)
	Female	115	(55)
Symptoms for at least 6 months	Abdominal discomfort	149	(71)
	Recurrent upper abdominal pain	86	(41)
	Vomiting	76	(36)
	Weight loss	42	(20)
	Jaundice	40	(19)
	Liver pain	10	(5)
	Nausea	155	(74)
Serum total bilirubin elevated (≥1.2 mg/dL)		50	(24)
Serum carbohydrate antigen –199 elevated (>37 U/mL)		84	(40)
Serum liver enzyme elevated*		61	(29)
Serum carcinoembryonic antigen elevated (>3.4 ng/dL)		63	(30)
Coexisting stones		63	(30)
Surgical procedure (n=204)	Pancreatoduodenectomy	57	(28)
	Biliary duct resection only	47	(23)
	Hepatic resection only	35	(17)
	Hepatic and biliary duct resection	29	(14)
	Lobectomy	20	(10)
	Segmentectomy	12	(6)
	Cholecystectomy	4	(2)

Variables are presented as frequency (percentage) for constant data and mean±SD for continuous data. * Serum glutamic oxaloacetic transaminase: normal range: 10–40 U/L; Alanine aminotransferase normal range: 7–56 U/L. 2–3 times higher than the normal range was considered an elevated level.
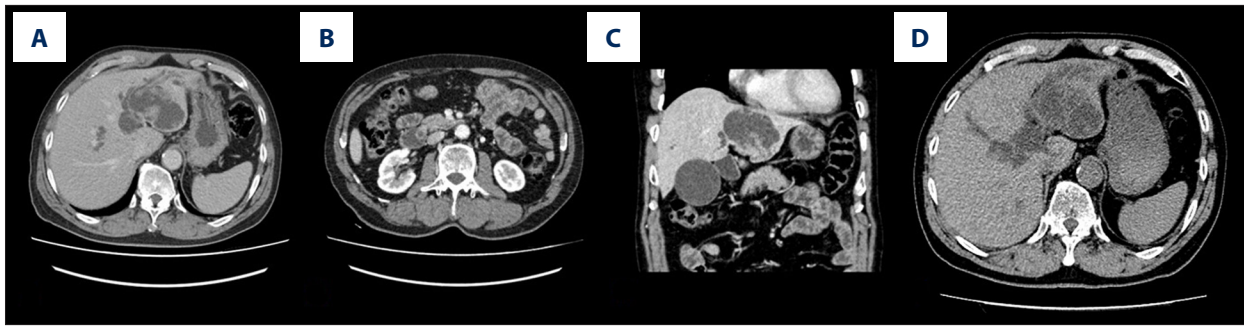
Figure 2. Computed tomography images of a male patient, age 67 years, with recurrent upper abdominal pain and the elevated serum liver enzyme level. Direct enhancement showed that the volume of the left lobe of the liver increased, and a solid non-uniform enhancement shadow was seen inside. The boundary was clear and the size was about 7.7×4.7 cm. The multiple wall nodules were enhanced and the lesion was connected with the left intrahepatic bile duct. There was no abnormal enhancement in the liver parenchyma. The bile duct and common bile duct were significantly expanded. The widest diameter of the common bile duct was about 3.3 cm. The gallbladder volume was increased, no abnormal density appeared in the gallbladder, and the pancreas and spleen were normal. No obvious abnormal enhancement shadows were observed. There was local aortic wall calcification. Sweeping and the left kidney views show a small circle of low-density, non-enhanced shadows, only a few millimeters in diameter, with no obvious enlarged lymph nodes after the retroperitoneum. No signs of ascites were found. (**A**) Liver left lobe cystic space-occupying lesion with intrahepatic bile duct and common bile duct dilatation, gallbladder enlargement, intraductal papillary myxoma (the contrast-enhanced axial view). (**B**) Aortic sclerosis (the contrast-enhanced axial view), (**C**) Left kidney small cyst (the contrast-enhanced sagittal view). (**D**) The non-enhanced axial view.
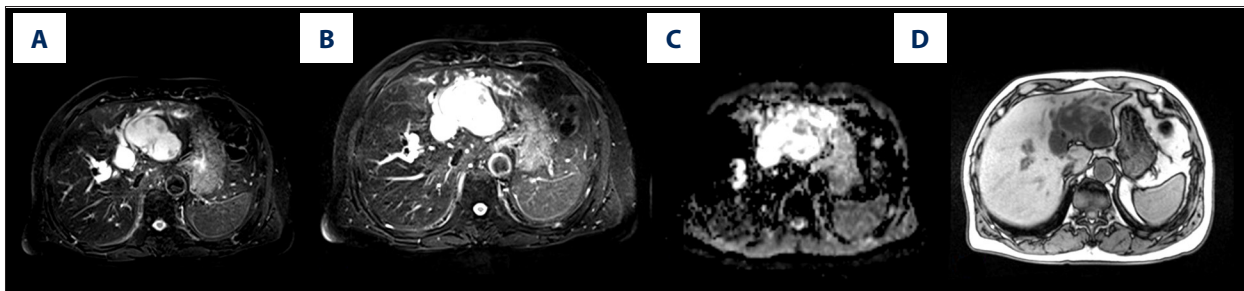
Figure 3. The axial view of magnetic resonance imaging of a male patient, aged 67 years, with recurrent upper abdominal pain and elevated serum liver enzyme level. The volume of the left lobe of the liver is increased, and a cystic solid abnormal signal is seen inside. It has a long T1 long T2 signal, and there are multiple nodular T2 signals, with the T1 slightly longer. The boundary is clear and the size is about 7.7×4.7 cm. After the enhancement, the solid part and the wall of the capsule were obviously enhanced. The lesion was connected with the left intrahepatic bile duct. There was no abnormal enhancement in the parenchyma of the remaining liver. The intrahepatic bile duct and common bile duct were obviously dilated. The wide diameter of the common bile duct was about 3.0 cm. The gallbladder volume was increased, no abnormal signal appeared in the gallbladder, there were no abnormalities in the morphology of the pancreas and spleen, and no obvious abnormal enhancement was observed. Sweeping and left kidney views show a small class of circular low signal without enhancement, only a few millimeters in diameter, with no obvious enlarged lymph nodes after the retroperitoneum. No signs of ascites were found. (**A**) T1-weighted, unenhanced view. (**B**) T2-weighted unenhanced view. (**C**) Diffused-weighted image, and (**D**) Contrast-enhanced view. Liver left lobe cystic space-occupying lesion with intrahepatic bile duct and common bile duct dilatation, gallbladder enlargement, and intraductal papillary myxoma. Left kidney small cyst.

Hepatic computed tomography findings

In CT images, direct enhancement showed clear boundaries of lobes of the liver and uniform enhancement of neoplasm inside the liver. The sizes of the nodules were predictable, and multiple nodules were connected with the intrahepatic bile duct. There was observable enhancement of liver parenchyma. The upstream and the downstream bile duct dilatation was also predictable. Spleen, pancreas, gall bladder, and kidney enhancements were visible (Figure 2).

Hepatic magnetic resonance imaging findings

In MRI, long T1-weighted and T2-weighted signals were found. The boundaries of liver lobes and the crimping of the liver capsule could be seen. It was easy to visualize neoplasms inside
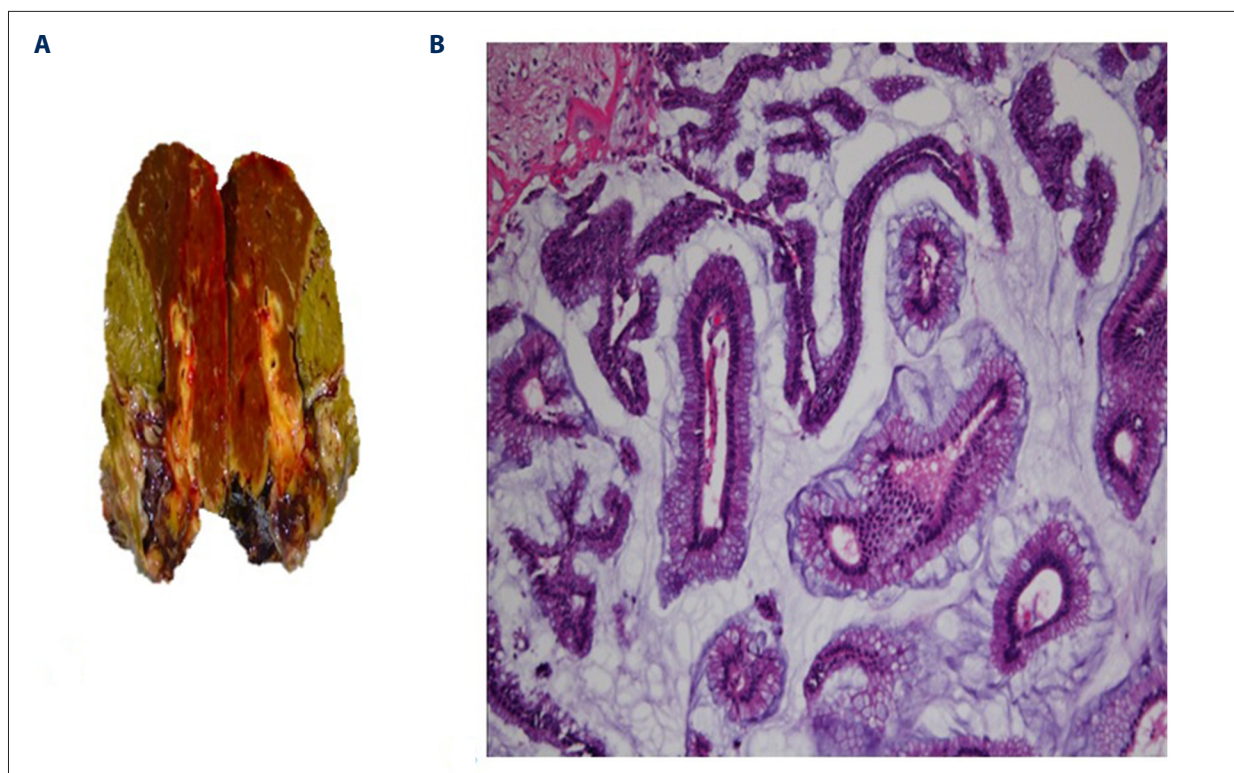
Figure 4. A surgical pathological analysis. (**A**) Gross appearance of the resected specimen. Intraductal papillary tumor, intestinal type, with low-grade dysplasia. The mass was approximately 0.1 cm from the leading edge of the liver. IHC: Ki67 (+, 30%), p53 (+, 10%), CK7 (small foci +), CK19 (+), CDX2 (+), MUC-1 (cavity +), Muc-2 (+), MUC5 (+), MUC6 (part +) (right half hepatectomy specimen). (**B**) Histopathology of hepatic lymph nodes of reactive hyperplasia of resected specimen (hematoxylin and eosin staining). Compared with the anterior piece, after drainage of the liver abscess, the drainage area was seen in the operation area, and the VII segment of the liver was seen as a lamellae low-density shadow, which was smaller than the front and had ring-shaped enhancement. During the operation, multiple morphological abnormalities were observed in the liver.

the liver, intrahepatic bile duct, spleen, pancreas, gall bladder, and kidney enhancement (Figure 3).

Pathological analysis

BT-ITPN was found in multiple solid tumor nodules at dilated bile ducts, without mucin production. Microscopically, they were seen to be polypoid tumor nodules (Figure 4).

Diagnostic parameters

CT images showed that a total of 171 out of 210 patients had BT-IPMN and 33 patients had BT-ITPN, but results were inconclusive for 6 patients. MRI images showed that 176 out of 210 patients had BT-IPMN and 28 patients had BT-ITPN, but results were inconclusive for 6 patients. Surgical procedures were performed for 204 out of 210 patients. Among these 204 patients, 179 had BT-IPMN and 25 had BT-ITPN. With reference to the surgical pathology, CT and MRI had more inconclusive results than the surgical pathology (p=0.03 for both). Nodule sizes detected by CT (p=0.259) and MRI (p=0.588) were

not significantly different from those reported by surgical pathology. CT and MRI both had the same accuracy (97.14% for both) for BT-IPMN. The sensitivities for diagnosis of BT-IPMN were 87.75%, 83.81%, and 81.43% for the surgical pathology, MRI, and CT, respectively. The detailed sensitivities and accuracies of the pathology of the surgical pathology, CT, and MRI for BT-IPMN are shown in Table 2.

Beneficial score analysis

Considering surgical pathology as the reference standard and working area to detect BT-IPMN at one time in images, CT had 0.32–0.92 diagnostic confidence and MRI had 0.125–0.955 diagnostic confidence, while at above 0.92 diagnostic confidence CT had the risk of overdiagnosis, and at above 0.955 diagnostic confidence MRI had the risk of overdiagnosis (Figure 5).
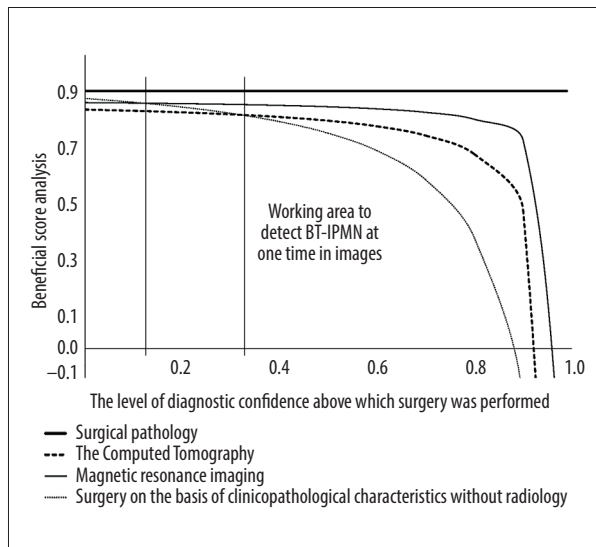
Intra-observer agreements

Intra-observer agreements for diagnosis of neoplasm were perfect (k=0.85), perfect (k=0.81), and substantial (k=0.79) for

Table 2. Parameters for diagnosis of biliary tract intraductal papillary mucinous neoplasm for imaging modalities.

Parameters	Surgical pathology	Imaging modalities			
		Computed tomography		Magnetic resonance imaging	
Data of patients included in the analysis	204	210	p-Value*	210	p-Value*
BT-IPMN	179 (88)	171 (81)	0.079	176 (84)	0.264
Inconclusive results	0 (0)	6 (3)**	0.030	6 (3)**	0.030
Sensitivities	87.75%	81.43%	0.248	83.81%	0.471
Accuracies	100.00%	97.14%	0.862	97.14%	0.862
Nodule size (mm)	13.54±3.12	13.92±3.69	0.259	13.71±3.25	0.588

Variables are presented as frequency (percentage) for constant data and mean±SD for continuous data. * With respect to the surgical pathology. BT-IPMN – biliary tract intraductal papillary mucinous neoplasm. The chi-square independence test was performed for categorical data and the Mann-Whitney U test was performed for continuous data. A p-value of less than 0.05 was considered significant. ** Significant difference with respect to the surgical pathology.

Figure 5. Beneficial score analysis.

surgical pathology, MRI, and CT, respectively. The detailed intra-observer agreements for location, numbers of lesions, and the size of neoplasm(s) are reported in Table 3.

Discussion

Non-invasive imaging modalities

In surgical pathology assessment, CT and MRI both had 97.14% accuracies for detection of BT-IPMN at one time in images. The results of the study were consistent with the results of previous retrospective analyses [6,8,13]. Endoscopic retrograde cholangiopancreatography, biliary tract endoscopy, duodenal endoscopy, and endoscopic ultrasound are available options for diagnosis of BT-IPMN [14], but these are invasive examinations that have high intra-observer variabilities and involve a risk of pancreatitis after the procedure [4]. Moreover, dilatation

Table 3. Intra-observer agreements for diagnostic parameters of imaging modalities.

Categories	Coefficient	Coefficient value		
		Surgical pathology	Imaging modalities	
			Computed tomography	Magnetic resonance imaging
Diagnosis of neoplasm	k	0.85	0.79	0.81
BT-IPMN or BT-ITPN	k	1	0.95	0.96
Numbers of lesions	k	1	0.97	0.98
The size of neoplasm	ICC	1	0.91	0.94

BT-IPMN – biliary tract intraductal papillary mucinous neoplasm; BT-ITPN – biliary intraductal tubulopapillary neoplasms. k – $kappa$ coefficient (0.99–0.81: perfect agreement, 0.80–0.61: substantial agreement, 0.60–0.41: moderate agreement, 0.40–0.21: fair agreement, and 0.20–0.01: slight agreement). ICC – The intraclass correlation coefficient (1.00–0.91: excellent, 0.90–0.81: very good, and 0.80–0.71: good).

of the bile duct is not possible to depict with these invasive techniques [8]. CT and MRI both have clinical importance in the diagnosis of BT-IPMN in patients with suspicious results of physical examinations and clinic-pathological features.

Computed tomography *vs.* magnetic resonance imaging

MRI had a higher working area to detect BT-IPMN at one time in images than did CT (0.125–0.955 *vs.* 0.32–0.92), but both had less risk of overdiagnosis. The differential diagnosis of biliary tract neoplasms is difficult [7]. BT-IPMN and BT-ITPN both require surgeries [6]. However, treatment options are different for BT-IPMN and the other neoplasms. MRI may have high sensitivity for the diagnosis of BT-IPMN.

Intra-observer agreements

Intra-observer agreements for diagnosis through the pathology of surgical pathology and MRI had a perfect agreement but CT had a substantial agreement. The results of the study were consistent with the results of previous retrospective analyses [5–7]. MRI can depict BT-IPMN as lesions with high intraductal soft tissue proportion without mucin production [5]. CT overestimates BT-IPMN lesions during diagnosis [7] because biliary neoplasms have a large amount of mucin [13] and mucin shows water signal intensity, which is difficult to diagnose by CT [5]. Gadopentetate dimeglumine-enhanced MRI can detect mucinous neoplasm of bile as hyperintense bile [4,15]. Also, T-2 weighted images can differentiate BT-IPMN from mucin [8]. MRI may be more reliable for the diagnosis of BT-IPMN, and CT results should be carefully evaluated in the diagnosis of patients with suspected biliary neoplasm.

Inconclusive results

CT and MRI both had 6 inconclusive results. Invasive bile duct neoplasms cannot be diagnosed by contrast-enhanced CT and contrast-enhanced MRI [16]. Gadopentetate dimeglumine is not taken up by neoplasms, but instead is absorbed by normal tissues; therefore, it is possible that contrast-enhanced MRI would yield inconclusive results, but in liver neoplasms, liver parenchyma and neoplasm would appear the same [4]. If contrast-enhanced MRI fails to provide adequate information, FDG PET/CT (fluorodeoxyglucose/positron emission tomography/computed tomography) is the preferred modality.

Limitations

This study has several limitations. This was a retrospective analysis, not a dynamic prospective study. However, prospective study of the differential diagnosis of BT-IPMN and BT-ITPN is difficult [5]. Postoperative MRI and CT were evaluated (data are not shown) to confirm the efficacy of the surgical procedure. The lower part of the common bile duct found to be abnormal and the residual pancreatic duct was slightly dilated in some patients in postoperative images. The cause of this abnormality was not discussed in the study. Also, treatment in the follow-up period was not discussed.

Conclusions

CT and MRI both have clinical importance in the diagnosis of biliary tract intraductal papillary mucinous neoplasm in patients with suspected biliary neoplasms. Our results suggest that MRI is more accurate and reliable than CT in assessment of biliary tract intraductal papillary mucinous neoplasms.

Acknowledgments

Availability of data and materials

The datasets used and analyzed in this study are available from the corresponding author on reasonable request.

Conflict of interest

None.

References:

1. Barton JG, Barrett DA, Maricevich MA et al: Intraductal papillary mucinous neoplasm of the biliary tract: A real disease? HPB, 2009; 11: 684–91

2. Wang X, Cai YQ, Chen YH, Liu XB: Biliary tract intraductal papillary mucinous neoplasm: Report of 19 cases. World J Gastroenterol, 2015; 21: 4261–67

3. Rocha FG, Lee H, Katabi N et al: Intraductal papillary neoplasm of the bile duct: A biliary equivalent to intraductal papillary mucinous neoplasm of the pancreas? Hepatology, 2012; 56: 1352–60

4. Ying SH, Teng XD, Wang ZM et al: Gd-EOB-DTPA-enhanced magnetic resonance imaging for bile duct intraductal papillary mucinous neoplasms. World J Gastroenterol, 2015; 21: 7824–33

5. Wu CH, Yeh YC, Tsuei YC et al: Comparative radiological pathological study of biliary intraductal tubulopapillary neoplasm and biliary intraductal papillary mucinous neoplasm. Abdom Radiol, 2017; 42: 2460–69

6. Liu Y, Zhong X, Yan L et al: Diagnostic performance of CT and MRI in distinguishing intraductal papillary neoplasm of the bile duct from cholangiocarcinoma with intraductal papillary growth. Eur Radiol, 2015; 25: 1967–74

7. Ogawa H, Itoh S, Nagasaka T et al: CT findings of intraductal papillary neoplasm of the bile duct: Assessment with multiphase contrast-enhanced examination using multi-detector CT. Clin Radiol, 2012; 67: 224–31

8. Takanami K, Yamada T, Tsuda M et al: Intraductal papillary mucinous neoplasm of the bile ducts: Multimodality assessment with pathologic correlation. Abdom Imaging, 2011; 36: 447–56

9. Kim HJ, Yu ES, Byun JH et al: CT differentiation of mucin-producing cystic neoplasms of the liver from solitary bile duct cysts. Am J Roentgenol, 2014; 202: 83–91

10. Da Ines D, Mons A, Braidy C et al: Hepatic capsular retraction: Spectrum of diagnosis at MRI. Acta Radiol Short Rep, 2014; 3: 2047981614545667

11. Minagawa N, Sato N, Mori Y et al: A comparison between intraductal papillary neoplasms of the biliary tract (BT-IPMNs) and intraductal papillary mucinous neoplasms of the pancreas (P-IPMNs) reveals distinct clinical manifestations and outcomes. Eur J Surg Oncol, 2013; 39: 554–58

12. Bierry G, Simeone FJ, Borg-Stein JP et al: Sacrotuberous ligament: Relationship to normal, torn, and retracted hamstring tendons on MR images. Radiology, 2014; 271: 162–71

13. Lim JH, Jang KT, Choi D: Biliary intraductal papillary-mucinous neoplasm manifesting only as dilatation of the hepatic lobar or segmental bile ducts: Imaging features in six patients. Am J Roentgenol, 2008; 191: 778–82

14. Kim KM, Lee JK, Shin JU et al: Clinicopathologic features of intraductal papillary neoplasm of the bile duct according to histologic subtype. Am J Gastroenterol, 2012; 107: 118–25

15. Lee NK, Kim S, Lee JW et al: MR appearance of normal and abnormal bile: Correlation with imaging and endoscopic finding. Eur J Radiol, 2010; 76: 211–21

16. Budzynska A, Hartleb M, Nowakowska-Dulawa E et al: Simultaneous liver mucinous cystic and intraductal papillary mucinous neoplasms of the bile duct: A case report. World J Gastroenterol, 2014; 20: 4102–5